



# 1 Characteristics of snowpack chemistry on the coastal region in the

# 2 northwestern Greenland Ice Sheet facing the North Water

- 3 Yutaka Kurosaki<sup>1</sup>, Sumito Matoba<sup>2</sup>, Mai Matsumoto<sup>2,3</sup>, Tetsuhide Yamasaki<sup>4</sup>, Ilannguaq Hendriksen<sup>5</sup>,
- 4 Yoshinori Iizuka<sup>2</sup>
- <sup>1</sup>Graduate School of Environmental Study, Nagoya University, Nagoya, 464-0813, Japan
- 6 <sup>2</sup>Institute of Low Temperature Science, Hokkaido University, Sapporo, 060-0819, Japan
- 7 <sup>3</sup>Graduate School of Environmental Science, Hokkaido University, Sapporo, 060-0810, Japan
- 8 <sup>4</sup>Avangnaq, Takatsuki 596-0094, Japan
- 9 <sup>5</sup>Siorapaluk, Avannaata Kommune, Greenland
- 10 Correspondence to: Yutaka Kurosaki (kurosaki.yutaka.g4@f.mail.nagoya-u.ac.jp),
- 11 Sumito Matoba (matoba@lowtem.hokudai.ac.jp)

#### 12 Abstract

13 In the North Water, the opening of sea ice due to polynya formation may influences the surrounding water and aerosol 14 circulation. We conducted glaciological observations from seacoast to inland on the western side of Prudhoe Land, which is 15 located in the northwestern Greenland Ice Sheet close to the North Water, to elucidate water and aerosol circulation around the North Water. The spatial variations in  $\delta^{18}O$  and chemical substances in surface snow showed that water vapor and aerosols 16 17 were directly transported from the southern North Water to northern inland of areas on the western side of Prudhoe Land. 18 Unlike the inland area of the Greenland Ice Sheet, the snowpack on the western side of Prudhoe Land contained signals of ocean biological and sea ice conditions in the North Water. The methanesulfonic acid identified in the summer snowpack 19 20 originated from a phytoplankton bloom in the North Water. NH<sub>4</sub><sup>+</sup> in autumn–winter snowpacks could originate from ammonia gas emissions from organisms in the North Water. The Na<sup>+</sup>, Cl<sup>-</sup>, K<sup>+</sup>, Mg<sup>2+</sup>, SO<sub>4</sub><sup>2-</sup>, and Ca<sup>2+</sup> concentrations in the snowpack 21 22 rapidly increased in winter, which could be attributed to the emission of frost flowers from the newly formed sea ice surface 23 into the atmosphere due to intense storm activity in the North Water. We suggest that the chemical substances identified in the 24 snowpack or ice core from the western side of Prudhoe Land can be used to better understand past changes in ocean biological 25 and sea ice conditions in the North Water.





#### 1 Introduction

26

27

28

29

30

31

32

33

34

35

36

37

38

39

40

41

42

43 44

45

46

47

48

49

50

51 52

53

54

55

56

57

58

The North Water (NOW) is one of the largest polynyas in the Arctic and is located between northwestern Greenland and Ellesmere Island in northern Baffin Bay (Barber and Massom, 2007) (Fig. 1a). The polynya in the NOW is formed by strong northerly winds from the Nares Strait and the supply of relatively warm Atlantic waters yielded by a branch of the West Greenland Current (Ito, 1982; Steffen and Ohmura, 1985; Mysak and Huang, 1992; Melling et al., 2001; Ingram et al., 2002; Dumont et al., 2009; Vincent, 2019). Polynya formation in the NOW supplies heat and moisture to the atmosphere and influences low-cloud formation around the NOW region. Monroe et al. (2021) reported that the low-cloud amount over polynyas can reach up to twice as high as that over nearby sea ice in the NOW. Moreover, polynya formation in the NOW influences ocean conditions such as vertical mixing by wind, the advection of nutrients into the euphotic layer, light availability, and density stratification. These physical factors enhance primary production and collectively support high levels of productivity in the NOW (Mei et al., 2002; Marchese et al., 2017). Additionally, the notable phytoplankton blooms promote the production of dimethylsulfides (DMS), and sea-to-air DMS emission contributes to marine cloud formation (e.g. Charlson et al., 1987). Sea ice fluctuations in the NOW influence not only water and aerosol circulation and ocean productivity but also human activities. The recent increase in the frequency of sea ice breakup in front of Siorapaluk village, which is the northernmost village in Greenland, influences hunting and fishing on sea ice and movement between villages on sea ice by dog sledges and skidoos in winter and spring (Matoba and Yamasaki, 2018). Decreases in the sea ice thickness and concentration in the NOW due to future climate warming could result in changes in water and aerosol circulation, ocean productivity, and human lifestyle conditions. To elucidate the changes in the source environmental conditions and the transport process of water vapor and aerosols over northwestern Greenland, snow pit and ice core observations have been conducted in the northwestern Greenland Ice Sheet (Kuramoto et al., 2011; NEEM Community members, 2013; Matoba et al., 2015; Matoba et al., 2018; Osterberg et al., 2015; Kurosaki et al., 2020). The chemical components and water stable isotopes in the snowpack on the Greenland Ice Sheet provide valuable information related to past changes in aerosol and water vapor conditions in source regions and their transport processes. Snow pit observations (NEEM; 77.45°N, 51.06°W, 2445 m above sea level (a.s.l.) (Fig. 1a)) at the inland of the northwestern Greenland Ice Sheet revealed seasonal variations in snowpack chemical compositions (Kuramoto et al., 2011). For example, the concentration of Ca2+ originating from mineral dust peaked from late winter to spring, the concentrations of SO<sub>4</sub><sup>2-</sup> and NO<sub>3</sub><sup>-</sup> originating from fossil fuel combustion peaked from winter to spring, and the concentration of MSA originating from marine phytoplankton peaked in spring and from late summer to autumn (Kuramoto et al., 2011). Analysis of mineral dust in an ice core from SIGMA-D (77.636°N, 59.120°W, 2100 m a.s.l.), which is located approximately 250 km from Qaanaaq on the northwestern coast of Greenland (Fig. 1a), revealed that the amount of local dust originating from the Greenland coastal region increased recently due to a decrease in snow cover during the warm season (Nagatsuka et al., 2021). Kurosaki et al, (2020) reported that the temporal variation in deuterium excess (d-excess) in an ice core from SIGMA-A (78.05°N, 67.63°W, 1490 m a.s.l.), which is located approximately 70 km northeast of Qaanaaq (Fig. 1a and b), was



72

73

74

75

76

77

78

79

80

81

82

83

84



59 significantly correlated with the sea ice concentration in northern Baffin Bay from 1979–2015. Via the use of relationship from 60 the SIGMA-A ice core, the temporal variation in sea ice concentrations over 100 years in northern Baffin Bay was 61 reconstructed (Kurosaki et al., 2020). Because all of these studies were performed at relatively high altitudes and far from the coast, the variations in chemical compositions and water stable isotopes were reflected by environmental changes in relatively 63 large areas driven by large-scale atmospheric circulation rather than local phenomena. Matoba et al. (2014) conducted multiple 64 snow pit observations at sites closer to the coast on the eastern side of Prudhoe Land, which is located the northern part of 65 Hayes peninsula in the northwestern Greenland facing the northeastern side of the NOW (Fig. 1a and b), and they reported notable spatial variations in water stable isotopes and chemical compositions at lower elevations and coastal regions. Water 66 67 vapor and sea salt on the glacier facing the ocean were transported from the coast, whereas water vapor, mineral dust, anthropogenic substances, and MSA on the eastern side of Prudhoe Land were transported from the west coast of Greenland 68 69 via the central part of the Greenland Ice Sheet (Matoba et al., 2014). The changes in the NOW could influence the water and 70 aerosol circulation in the northwestern Greenland. However, the past changes in the NOW have never been traced from the 71 previous snow and ice core observations in the northwestern Greenland Ice Sheet.

The western side of Prudhoe Land facing the northeastern side of the NOW is located between Inglefield Land in the north and the southern part of Hayes peninsula in the south (Fig. 1a and b). The Inglefield Land is dry area where the precipitation amount is quite low. On the other hand, the southern part of Hayes peninsula is one of the highest areas of precipitation amount (> 600 mm yr<sup>-1</sup>) in the northwestern Greenland due to the southerly moisture advection (Bales et al., 2001). The western side of Prudhoe Land, where locates between these regions with large contrast in precipitation, could be influenced by complicate processes of the heat and moisture supply from the ocean around this region including the NOW. However, most of meteorological and glaciological observations have been conducted on the southern part of Hayes peninsula in the northwestern Greenland (Bales et al., 2001; Osterberg et al., 2015; Becagli et al., 2016; Akers et al., 2020), not on Prudhoe Land. In order to make accurate future projections of environmental change in this region, where the influences of climate warming on the life activities in this region is already emerging, it is necessary to clarify the impact of changes in the NOW on the processes of the heat and moisture circulation in this region.

We conducted glaciological observations on the western side of Prudhoe Land facing the NOW to elucidate water and aerosol circulation around the NOW, which influences the environmental changes and related human activities in this region.





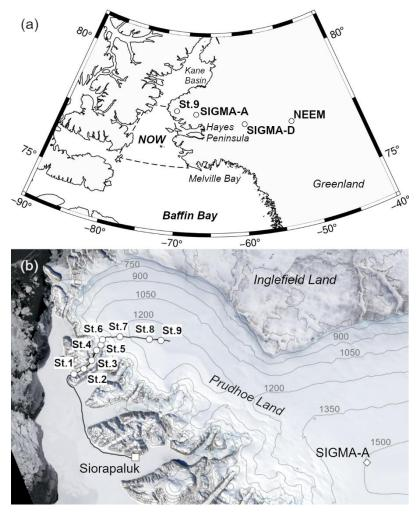


**Figure 1: Maps of the sampling sites.** (a) shows location of the snowpit and ice core sampling sites in this study (St. 9) and previous studies (SIGMA-A, SIGMA-D, and NEEM) in the northwestern Greenland Ice Sheet. The dashed polygon in (a) denotes the approximate location of the NOW. Hayes peninsula in the northwestern Greenland is located between Kane Basin in the north and Melville Bay in the south. (b) shows Landsat-8 image around St. 9 and SIGMA-A of Prudhoe Land, which is located on the northern part of Hayes peninsula, on 13 April 2023. The black circles in (b) denote the sampling sites from St. 1 to St. 9, and the black line denotes dog sledge route. The gray contours in (b) are drawn from the Greenland Mapping Project 2 (GIMP-2) Digital Elevation Model version 2.





#### 2 Methods

93

94

95

96

97

98

99

100101

102

103104

105

106

107

108109

110

111

112

113

114

115

116117

118119

120

121122

123

# 2.1 Observations and chemical analysis

We conducted snow observations from 9-11 April 2023 on the western side of Prudhoe Land, which is a coastal site in the northwestern part of the Greenland Ice Sheet (Fig. 1). The expedition base was established in Siorapaluk village at 77.78°N and 70.75°W. Siolapaluk village faces Robertson Fjord, which is located on the northeastern side of the NOW (Fig. 1b). The observation route is shown in Fig. 1b. We started from Siorapaluk on 9 April 2023 on dog sledges, moved on sea ice westward from Sioraparuk, climbed the Clements Glacier, and advanced on the Greenland Ice Sheet. We arrived at the terminal point of the route (78.13°N, 71.06°W, 1279 m above sea level (St. 9)) on 10 April 2023 and returned to Siorapaluk on 11 April 2023. We conducted glaciological observations along the route. The locations and elevations of the observation sites are shown in Fig. 1b and Fig. 2. We conducted snow pit observations on the glacier (St. 3) and the ice sheet (St. 9) along the route to measure the chemical species, stratigraphy, and density of the snowpack. Snow samples for chemical analysis at St. 3 and St. 9 were collected from the snow walls of the snow pit using a precleaned stainless-steel sampler into Whirl-Pak polyethylene bags (Nasco). The snow sampling intervals at St. 3 were 0.02 m from 0.00 to 0.20 m and 0.03 m from 0.20 to 1.01 m, and the snow sampling intervals at St. 9 were 0.02 m from 0.00 to 0.20 m and 0.03 m from 0.30 to 1.08 m. Additionally, an ice core was collected at St. 9 from 1.08 to 4.20 m using a hand corer. After the stratigraphy and density of the ice core were measured, the ice core samples were cut at 0.05-0.10 m intervals using a precleaned saw, were polished using a precleaned ceramic knife to remove contamination on the ice core samples and were then placed into Whirl-Pak polyethylene bags. Surface snow samples for chemical analysis were also collected at 9 sites along the route using a precleaned stainless-steel sampler into Whirl-Pak polyethylene bags. The snow samples were kept frozen and were transported to Siorapaluk. The snow samples were melted at ambient temperature, were placed in 50 mL clean polypropylene bottles, and were then kept frozen in a portable freezer (approximately -18 °C). The samples were then transported to a cold room (-20 °C) at the Institute of Low Temperature Science (ILTS) of Hokkaido University, Japan, and were then kept frozen until chemical analysis. The concentrations of Na<sup>+</sup>, NH<sub>4</sub><sup>+</sup>, K<sup>+</sup>, Mg<sup>2+</sup>, Ca<sup>2+</sup>, methane sulfonate (hereafter referred to as MSA), Cl<sup>-</sup>, SO<sub>4</sub><sup>2-</sup>, and NO<sub>3</sub> were measured by ion chromatography (ICS-2100, Thermo Scientific). We used a Dionex CS12-A column with 20 mM MSA eluent and a Dionex AS-18 column with 23 mM KOH eluent for cation and anion measurements, respectively. The analytical precision of the ion chromatography was < 5 % (at the measurement of 20 ppb standard). The limit of detection was < 0.1 ppb. The limit of quantification was < 0.5 ppb. The samples exhibiting large peak were measured multiple times, to confirm that any large peak in ion concentration was not caused by analytical errors. The stable oxygen and hydrogen isotopic compositions of the water samples were measured by a water stable isotopes analyzer (L2130-I, Picarro Inc.) with an evaporating device (A0211, Picarro Inc.). The analysis precisions for  $\delta^{18}O$  and  $\delta D$  were 0.08% and 0.8%, respectively.





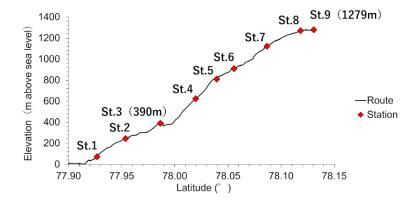


Figure 2: Elevation above sea level of each station.

### 2.2 Meteorological and sea ice data

We used meteorological and sea ice data from northwestern Greenland and Baffin Bay to analyze the factors contributing to the variations in chemical species and water stable isotopes in snow on the northwestern coast of Greenland. The temperature, relative humidity, wind speed, wind direction, and atmospheric pressure at Siorapaluk were measured by an automatic weather station (AWS) (WXT530, Vaisala) from April 2021 to March 2024 (Matoba et al., 2024). The AWS was installed 2 m above ground level (a.g.l.), and these meteorological factors were observed at 10-minutes intervals. We also used data of the air temperature, geopotential height, wind speed, and wind direction around the northwestern coast of Greenland and Baffin Bay from ERA5 reanalysis dataset supplied by the European Center for Medium Range Weather Forecasts (ECMWF) (Hersbach et al., 2020).

### 3 Results and Discussion

# 3.1 Snowpack dating and annual accumulation

The snowpack at St. 3 and St. 9 was dated on the basis of the snow stratigraphy and seasonal variations in  $\delta^{18}$ O, d-excess (d-excess =  $\delta D - 8\delta^{18}$ O) and MSA. The vertical profiles of the snow stratigraphy at St. 3 and St. 9 are shown in Fig. 3. Rounded grains, faceted crystals, and depth hoars were observed from 0.00 to 1.01 m in the glacier at St. 3 (Fig. 3a). Glacier ice was present below 1.01 m at St. 3. The snowpack from 0.00 to 1.01 m at St. 3 corresponds to seasonal snow for the periods from autumn in 2022 to spring in 2023. Rounded grains, faceted crystals, and depth hoars were observed from 0.00 to 0.96 m at St. 9 (Fig. 3b). Below 0.96 m at St. 9, melt forms prevailed, and some ice layers with thickness ranging from several millimeters

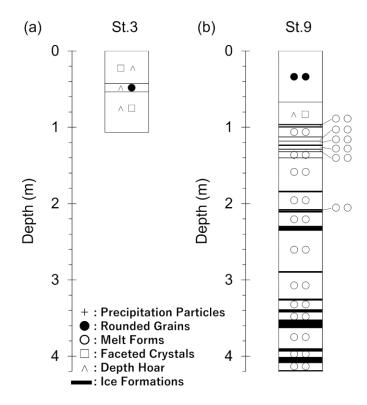




to 10 cm were found (Fig. 3b). The ice layers indicated that the surface or subsurface of the snowpack melted in summer. 144 Therefore, we assumed that the depth of 0.96 m at St. 9 corresponds to the end of summer in 2022. Vertical profiles of  $\delta^{18}$ O, 145 d-excess and MSA at St. 9 are shown in Fig. 4. The seasonal variation in  $\delta^{18}$ O reflects the air temperature and exhibits a 146 147 maximum value in summer and a minimum value in winter at several Greenland sites (Steffensen et al., 1988; Legrand and Mayewski, 1997; Kuramoto et al., 2011; Kurosaki et al., 2020; Nakawaza et al., 2021). The seasonal variation in d-excess 148 reflects the sea surface temperature and sea-to-air evaporation process in the water vapor source region of precipitation 149 150 (Merlivat and Jouzel, 1979; Uemura et al., 2007; Kurita, 2011; Kopec et al., 2019). At several sites in Greenland, the d-excess 151 of snowpack exhibits maximum values in autumn and minimum values from spring to early summer (Johnsen et al., 1989; 152 Kuramoto et al., 2011). MSA is an oxidization product from dimethyl sulfide (DMS), which originates from ocean 153 phytoplankton. The seasonal variation in MSA exhibits maximum values from spring to summer during ocean phytoplankton 154 blooms and minimum values in winter (Jaffrezo et al., 1994; Legrand and Mayewski, 1997; Kuramoto et al., 2011; Osterberg et al., 2015; Nakazawa et al., 2021; Kurosaki et al., 2022). At St.9, the  $\delta^{18}$ O value decreased from 0.04 m, negatively peaked 155 at 0.13 m and increased toward 0.87 m (Fig. 4a). The d-excess value increased from 0.00 m, peaked positively at 0.51 m and 156 157 decreased toward 1.08 m (Fig. 4b). The MSA concentration was below the detection limit or exhibited low-values from 0.00 to 0.72 m and substantially increased from 0.72-1.15 m (Fig. 4c). Consequently, we determined the seasonality from 0.00 to 158 159 1.15 m as shown below. The snow layers from 0.00-0.04 m accumulated close to the observation date (April 2023), the snowpack in 0.04–0.72 m corresponded to the autumn to winter period from 2022–2023, resulting in the negative  $\delta^{18}$ O peak, 160 positive d-excess peak and low MSA values. The snowpack from 0.72 m-1.15 m corresponded to spring to summer in 2022, 161 resulting in ice layer formations, high  $\delta^{18}$ O value and high MSA values. Below 0.96 m, the seasonal amplitudes of  $\delta^{18}$ O and 162 d-excess were smaller than those in the shallower layers from 0.00-0.96 m because of summer melting (Fig. 4a). Even though 163 164 the values of the water stable isotopes were smoothed by summer melting and some chemical species showed high peaks in 165 the ice layers owing to relocation processes by meltwater refrozen below 0.96 m, the MSA concentration showed obvious seasonal variations, and the  $\delta^{18}$ O values exhibited slight seasonal variations (Fig. 4a and c). We assigned the snow layers with 166 high MSA and  $\delta^{18}$ O values to the spring to summer period and assigned the snow layers with low MSA and  $\delta^{18}$ O values to 167 168 autumn to winter period. Consequently, the firn layers from 1.15-1.45 m, 2.02-2.28 m, and 3.12-3.39 m corresponded to the autumn-winter periods from 2021-22, 2020-21, and 2019-20, respectively. The snowpacks from 1.45-2.02 m and 2.28-3.12 169 m corresponded to the spring-summer periods in 2021 and 2020, respectively. According to the snowpack dating approach 170 171 described above, the annual accumulation rates at St. 9 were 0.42±0.13 m w.eq. yr<sup>-1</sup> and 0.56±0.11 m w.eq. yr<sup>-1</sup> from winter 172 2021 to winter 2022 and from winter 2020 to winter 2021, respectively. The snow density used for calculation the annual accumulation rate was 492 kg m<sup>-3</sup> which is the average of the ice core from 1.10-3.28 m at St. 9. The Fifth Generation 173 174 Mesoscale Model modified for polar climates (Polar MM5) using firn core and meteorological station data estimated that the 175 climatological value of the annual accumulation rate on the inland of the western side of Prudhoe Land ranged from 0.31–0.43 176 m w.eq. yr<sup>-1</sup> for the 1958–2007 period (Burgess, et al., 2007). The annual accumulation rate derived from the snowpack at St. 177 9 in this study was comparable to or slightly higher than the climatological value.







179

Figure 3. Vertical profiles of the physical stratigraphy at (a) St.3 and (b) St.9.



184185

186

187

194

195 196



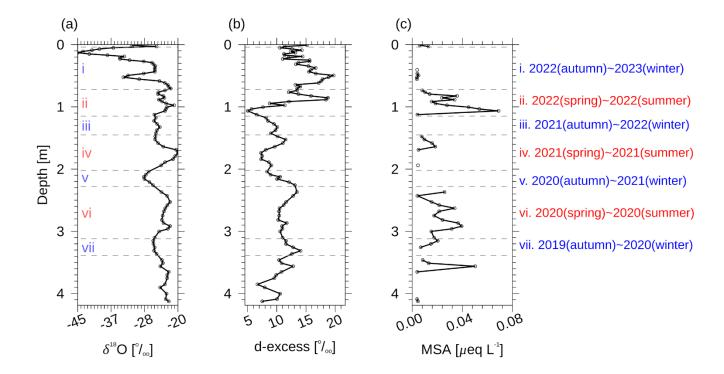


Figure 4. Vertical profiles of (a)  $\delta^{18}$ O, (b) d-excess, and (c) MSA at St. 9. i–vi denote the seasons from 2019 to 2023. i, iii, v, and vii denote autumn to winter period from 2022–2023, 2021–2022, 2020–2021, and 2019–2020, respectively. ii, iv, and vi denote spring to summer period in 2022, 2021, and 2020, respectively.

#### 3.2 Spatial and temporal variations in water stable isotopes and chemical species

The  $\delta^{18}O$  and concentrations of ions species (Na<sup>+</sup>, NH<sub>4</sub><sup>+</sup>, K<sup>+</sup>, Mg<sup>2+</sup>, Ca<sup>2+</sup>, Cl<sup>-</sup>, SO<sub>4</sub><sup>2-</sup>, MSA, and Cl<sup>-</sup>/Na<sup>+</sup>) in surface snow are shown in Fig. 5. Vertical profiles of  $\delta^{18}O$  at St. 3 and St. 9 are shown in Fig. 6, and vertical profiles of the concentrations of the ion species at St. 3 and St. 9 are shown in Fig. 7 and Fig. 8, respectively. The non-sea-salt (nss) components of K<sup>+</sup>, Mg<sup>2+</sup>, Ca<sup>2+</sup>, and SO<sub>4</sub><sup>2-</sup> were calculated using the seawater ratios of these ions with respect to Na<sup>+</sup>, thereby assuming that Na<sup>+</sup> is solely of a sea-salt origin. For example, the concentration of nssSO<sub>4</sub><sup>2-</sup> was calculated following Eq. (1):

193 
$$[nssSO_4^{2-}] = [SO_4^{2-}] - (SO_4^{2-}/Na^+)_{sea} \times [Na^+],$$
 (1)

We applied the concentration unit as  $\mu$ eq  $L^{-1}$ . The  $(SO_4^{2-}/Na^+)_{sea}$  is the equivalent concentration ratio of  $SO_4^{2-}/Na^+$  in the sea water, which is 0.12. Similarly, the concentrations of  $nssK^+$ ,  $nssMg^{2+}$  and  $nssCa^{2+}$  were calculated using sea water ratios of 0.021, 0.23, and 0.044, respectively (Wilson, 1975; Legrand and Mayewski, 1997).



197

198

199 200

201

202 203

204 205

206

207

208

209 210

211

212

213

214

215 216

217

218

219

220

221

222

223

224



The spatial variations in  $\delta^{18}$ O in the surface snow showed maximum and minimum values at St. 3 (-19.12 ‰) and St. 9 (-37.21 %), respectively. The average  $\delta^{18}$ O value from 0.00 to 1.01 m at St. 3 was greater than that at St. 9 (St. 3: -22.03 %; St. 9: -29.12 %) (Table 1). The  $\delta^{18}$ O values in surface snow and the snowpack decreased from the seacoast toward the inland site (Fig. 5a and Table 1). We suggest that the spatial variation in the  $\delta^{18}$ O results from water vapor transport from the southern coast to the northern inland area by southerly winds. On the other hand, Matoba et al. (2014) reported different spatial variations in  $\delta^{18}$ O in surface snow on the eastern side of Prudhoe Land. The  $\delta^{18}$ O value of surface snow on the northwestern coast of Greenland decreased along the elevation on a glacier from sea level to 1,100 m a.s.l. and increased toward the inland on the Greenland Ice Sheet. Matoba et al. (2014) suggested that the distribution of  $\delta^{18}$ O values in surface snow resulted from the water vapor pathway, which originates from southern Baffin Bay, after which it first progress toward the northeast and then moves the inland of the Greenland Ice Sheet, and if finally turns northwest on the western coast of Greenland because of the cyclonic flow into a depression at Melville Bay. Because the observation site in this study is located in the westernmost part of Prudhoe Land, it is not affected by water vapor passing through the interior of the Greenland Ice Sheet, and water vapor transport from the south mainly influences the spatial variation in  $\delta^{18}$ O.

The vertical profile of  $\delta^{18}$ O in the snowpacks at St. 9 was similar to that at St. 3. The depths of the negative and positive peaks of  $\delta^{18}$ O at St. 9 agreed well with those at St. 3, and the vertical profile of  $\delta^{18}$ O between 0.00 and 1.01 m at St. 9 correlated significantly with that at St. 3 (r = 0.69, p < 0.01). Therefore, we propose that the snowpack corresponding to autumn–winter from 2022-2023 at St. 3 and St. 9 at the same snow depth accumulated with precipitation attributed to the same snowfall events, and  $\delta^{18}$ O in the snowpack had not been changed by the post depositional processes, which is water molecule diffusion, wind blowing, and sublimation. The difference in  $\delta^{18}$ O values between St. 3 and St. 9 increased from summer to winter from 2022–2023 and decreased until spring in 2023 (Fig. 6c). Matoba et al. (2002) reported that the  $\delta^{18}$ O values of precipitation in Siorapaluk was positively correlated with the surface air temperature. We suggest that the altitude gradient of the surface air temperature in winter was greater than that in summer in the western region of Prudhoe Land.

The possible sources of Na<sup>+</sup> and Cl<sup>-</sup> are sea salt and frost flowers (Legrand and Mayewski, 1997). The Na<sup>+</sup> and Cl<sup>-</sup> concentrations in surface snow decreased with increasing distance from the seacoast (Fig. 5b and g). The average values of Na<sup>+</sup> and Cl<sup>-</sup> between 0.00 and 1.01 m at St. 3 were four times greater than those at St. 9 (Table 1). Positive peaks of these ions at St. 9 were found from autumn-winter (Fig. 8a and f). The spatial variations in Na<sup>+</sup> and Cl<sup>-</sup> in surface snow were similar to those in the eastern region of Prudhoe Land (Matoba et al., 2014). The Na<sup>+</sup> and Cl<sup>-</sup> concentrations at several sites in the inland of the Greenland Ice Sheet also exhibit maximum values in winter (Steffensen, 1988; Fischer and Wagenbach, 1996; Dibb et al., 2007; Kuramoto et al., 2011).

225

226 The Na<sup>+</sup> and Cl<sup>-</sup> concentrations in snow are modified with respect to the bulk seawater composition due to heterogeneous 227 reactions with atmospheric acids such as H<sub>2</sub>SO<sub>4</sub> and HNO<sub>3</sub> (Cadle, 1972; Delmas et al., 1982; Kerminen et al., 2000):

228 
$$2\text{NaCl} + \text{H}_2\text{SO}_4 \rightarrow \text{Na}_2\text{SO}_4 + 2\text{HCl},$$
 (R1)

$$229 \quad \text{NaCl} + \text{HNO}_3 \rightarrow \text{NaNO}_3 + \text{HCl}, \tag{R2}$$





230 Na<sub>2</sub>SO<sub>4</sub> and NaNO<sub>3</sub> are removed from the atmosphere through the rainout process following the formation of cloud 231 condensation nuclei and precipitation. Therefore, the Cl<sup>-</sup>/Na<sup>+</sup> ratio often reveals sea salt modification within the atmosphere. 232 In general, if sea-salt is transported for a long time in the atmosphere, Na+ is scavenged to a greater degree than Cl- due to 233 reactions with  $H_2SO_4$  and  $HNO_3$ , and  $Cl^-/Na^+$  is thus higher than the sea-water ratio (1.17). The  $Cl^-/Na^+$  ratio in the snowpack 234 at St. 9 was close to the seawater ratio for all seasons (Fig. 8j). Additionally, the values of Cl<sup>-</sup>/Na<sup>+</sup> in the snowpack at St. 3 235 and in surface snow at all the sites were close to the seawater ratio (Fig. 5k and Fig. 7j). At several sites in the northwestern 236 Greenland Ice Sheet, Cl<sup>-</sup>/Na<sup>+</sup> exhibited maximum values in summer (Kuramoto et al., 2011; Kurosaki et al., 2020). In contrast, 237 the Cl<sup>-</sup>/Na<sup>+</sup> ratio at St.9 did not show clear seasonality. Therefore, the sea salt observed in this study could be transported along 238 a short-distance pathway without reactions with H<sub>2</sub>SO<sub>4</sub> and HNO<sub>3</sub> in the atmosphere throughout the year, and the possible 239 source region is the NOW polynya. 240 The possible source of nssK<sup>+</sup> and NH<sub>4</sub><sup>+</sup> is biomass burning (Fuhrer and Legrand, 1997; Legrand and Mayewski, 1997; 241 Kuramoto et al., 2011). The concentration of nssK<sup>+</sup> in surface snow did not change from St. 1 to St. 9 (Fig. 5d) and did not 242 show clear seasonality in the snowpack at St. 3 and St. 9 (Fig. 7c and Fig. 8c). NH<sub>4</sub><sup>+</sup> in surface snow reached maximum values 243 at St. 5 (Fig. 5c). NH<sub>4</sub><sup>+</sup> in the snowpack at St. 3 and St. 9 exhibited minimum values from spring–summer and maximum values 244 from autumn-winter (Fig. 7b and Fig. 8b). Positive peak values of NH<sub>4</sub><sup>+</sup> were exhibited at depths of 1.38, 2.04, and 3.31 m 245 corresponding to autumn-winter periods from 2021-2022, 2020-2021, and 2019-2020, respectively (Fig. 8b). At several sites 246 in the inland of the Greenland Ice Sheet, the concentration of NH<sub>4</sub><sup>+</sup> peaked from spring-summer owing to biomass-burning 247 events (Dibb et al., 2007; Nakazawa et al., 2021; Kjær, et al., 2022). In contrast, the concentrations of NH<sub>4</sub><sup>+</sup> at St. 9 did not 248 peak in spring-summer. The autumn-winter maximum of NH<sub>4</sub><sup>+</sup> at St. 3 and St. 9 have not been observed at the inland sites of the Greenland Ice Sheet. According to an incubation experiment of nitrogen-fixing organisms using artificial seawater, a 249 250 substantial increase in the atmospheric emission of ammonia gas and gas-phase basic water-soluble organic nitrogen (WSON) 251 was found during the decline and death phases of the organisms (Dobashi, 2023). The NOW polynya facing our study sites is 252 one of the most biologically productive marine areas of the Arctic Ocean (Klein et al., 2002; Odate et al., 2002). Phytoplankton 253 blooms in the NOW onsets in April, are sustained for three months, and then decline and death from autumn-winter (Mei et 254 al., 2002; Marchese et al., 2017). We suggest that the increase in NH<sub>4</sub><sup>+</sup> in the snowpack at St. 3 and St. 9 from autumn–winter 255 was caused by the increase in sea-to-air emission of ammonia gas during the decline and death phases of phytoplankton in the 256 NOW polynya. 257 The possible source of nssMg<sup>2+</sup> and nssCa<sup>2+</sup> is terrestrial dust (Dibb et al., 2007; Kuramoto et al., 2011). In surface snow, the maximum value of nssCa<sup>2+</sup> occurred at St. 2, while nssMg<sup>2+</sup> did not exhibit spatial variation (Fig. 5e and f). The nssMg<sup>2+</sup> 258 259 and nssCa<sup>2+</sup> concentrations in the snowpack at St. 9 peaked in spring (at a 1.07 m depth) and summer (at depths of 0.89 and 260 1.53 m) in 2021 and 2022 (Fig. 8d and e). In the inland areas of the Greenland Ice Sheet, mineral dust, which originates mainly 261 from Asia and North Africa (hereafter referred to as remote dust), was observed in spring layers in snowpacks or ice cores 262 (Steffensen et al., 1988; Whitlow et al., 1992; Mosher et al., 1993; Drab et al., 2002; Kuramoto et al., 2011; Nakazawa et al., 263 2021; Nagatsuka et al., 2021). The spring peaks of nssMg<sup>2+</sup> and nssCa<sup>2+</sup> in the snowpack at St. 9 could have originated from



264265

266

267

268

269270

271

272

273

274

275

276277

278

279

280

281

282

283

284285

286

287288

289

290291

292

293

294

295296



remote dust. However, the summer peaks of nssMg<sup>2+</sup> and nssCa<sup>2+</sup> in the snowpack at St. 9 have not been observed in the inland of the Greenland Ice Sheet. Recently, the decreasing snow cover area in the Arctic associated with Arctic warming, which is processing at a rate two to four times faster than the global average, has increased mineral dust emissions from bare land in the Arctic during the summer–autumn period (hereafter referred to as local dust) (Amino et al., 2020; Matsui et al., 2024). We assumed that the summer peaks of nssMg<sup>2+</sup> and nssCa<sup>2+</sup> in the snowpack at St. 9 could be attributed to local dust on the northwestern coast of Greenland.

The possible sources of NO<sub>3</sub><sup>-</sup> are fossil fuel combustion, biogenic soil emission, biomass burning, and photochemical reactions due to lightning (Legrand and Mayewski, 1997; Hastings et al., 2004). The concentration of NO<sub>3</sub><sup>-</sup> in surface snow on Clements Glacier decreased with increasing distance toward the top of the glacier (Fig. 5h). The average concentrations of NO<sub>3</sub> at depths from 0.00–1.01 m at St. 3 were greater than that at St. 9 (Table 1). The decreasing trend with distance from the seacoast was similar to that in the eastern region of Prudhoe Land (Matoba et al. 2014). The positive peak of NO<sub>3</sub><sup>-</sup> at St. 3 was observed on the snow surface corresponding to the spring of 2023 (Fig. 7g). The concentrations of NO<sub>3</sub><sup>-</sup> at St. 9 showed several positive peaks at depths of 0.01, 1.07, 1.94, 2.37, 2.87, 3.15, and 3.57 m (Fig. 8g). According to the stratigraphy of the snowpack at St. 9, we attributed the peaks at 0.01, 1.07, 1.94 and 3.15 m to the deposition of atmospheric nitrate and the peaks at 2.37, 2.87 and 3.57 m to melting and refreezing process. The seasonal variations in the snowpack at St. 3 and St. 9 exhibited maximum values from winter-spring and low values in summer, excluding positive peaks in the ice layers. At several inland sites in Greenland, positive peaks of NO<sub>3</sub><sup>-</sup> occurred in summer and from winter–spring (Kuramoto et al., 2011; Oyabu et al., 2016; Nakazawa et al., 2021). On the basis of the seasonal variation in the nitrogen and oxygen isotopes of NO<sub>3</sub><sup>-</sup> in the snowpack at Summit, the source of NO<sub>3</sub><sup>-</sup> in summer is natural NO<sub>x</sub> produced by biomass burning, biogenic soil emissions, and photochemical reactions due to lightning, whereas that in winter is anthropogenic NO<sub>x</sub> from fossil fuel combustion (Hastings et al., 2004). We assumed that the snowpack at St. 3 and St. 9 included aerosols originating from fossil fuel combustion and did not include aerosols originating from biomass burning, unlike the inland sites in Greenland.

The possible sources of nssSO<sub>4</sub><sup>2-</sup> are volcanic eruption, fossil fuel combustion, mineral dust, and DMS emissions produced by marine phytoplankton (Jaffrezo et al., 1994; Legrand and Mayewski, 1997). The concentrations of nssSO<sub>4</sub><sup>2-</sup> in surface snow increased from St. 1 to St. 9 (Fig. 5i). The increasing trend with distance from the seacoast was similar to that in the eastern region of Prudhoe Land (Matoba et al. 2014). The concentrations of nssSO<sub>4</sub><sup>2-</sup> at St. 9 showed several positive peaks at depths of 0.01, 1.04, 1.94, 2.37, 2.68, 2.87, 2.96, and 3.57 m (Fig. 8h). According to the stratigraphy of the snowpack at St. 9, we attributed the peaks at 0.01, 1.04, 1.94, 2.68 and 2.96 m to the deposition of atmospheric sulfate and the peaks at 2.37, 2.87 and 3.57 m to melting and refreezing process (Fig. 8h). The seasonal variations in the snowpack at St. 3 and St. 9 peaked from winter–spring and summer, excluding positive peaks in the ice layers. At several sites in Greenland, nssSO<sub>4</sub><sup>2-</sup> exhibited maximum values from winter–spring, which is attributed to anthropogenic fossil fuel combustion (Dibb et al., 2007; Kuramoto et al., 2011; Oyabu et al., 2016). Therefore, we believe that the source of positive nssSO<sub>4</sub><sup>2-</sup> peaks from winter–spring at St. 9 could be fossil fuel combustion, such as that at the inland sites in Greenland.



297

298

299300

301

302

303

304305

306307

308

309310

311

312

313

314

315

316

317318



Several negative nssSO<sub>4</sub><sup>2-</sup> peaks were found from autumn-winter in the snowpack at St. 3 and St. 9 (Fig. 7h and Fig. 8h). In a coastal Antarctic ice core, negative peaks have also been observed. The negative values of nssSO<sub>4</sub><sup>2-</sup> in the snowpack result from the low SO<sub>4</sub><sup>2-</sup>/Na<sup>+</sup> in aerosols emitted from frost flowers on newly formed sea ice (Rankin et al., 2002; Woolf et al., 2003; Rankin et al., 2004). Frost flowers are depleted in sulfate relative to sodium owing to the precipitation of mirabilite (Na<sub>2</sub>SO<sub>4</sub>10H<sub>2</sub>O) during the formation of sea ice at temperatures below -8 °C (Richardson, 1976; Rankin et al., 2000; Rankin et al., 2002; Hara et al., 2017). In northwestern Greenland, the frost flowers collected from newly formed sea ice in front of Siorapaluk indicated depletion in sulfate relative to that in seawater (Hara et al., 2017). The negative  $nssSO_4^{2-}$  peaks observed at our study sites could be attributed to the atmospheric emission of frost flowers from newly formed sea ice in the NOW polynya, where new sea ice is often created and broken up by strong northerly winds in winter. MSA is an oxidation product of DMS, which originates from ocean phytoplankton (Charlson et al., 1987; Jaffrezo et al., 1994). The concentration of MSA in surface snow reached a maximum value at St. 6 (Fig. 5j). The concentration of MSA in the snowpack was extremely high at 1.01 m at St. 3, corresponding to the summer of 2022 (Fig. 7i). The concentrations of MSA at St. 9 showed several positive peaks at depths of 0.83, 1.07, 1.64 2.37, 2.68, 2.91, and 3.57 m (Fig. 8i). According to the stratigraphy of the snowpack at St. 9, we attributed the peaks at 0.83, 1.07, 1.64, and 2.68 m to the deposition of atmospheric MSA and the peaks at 2.37, 2.91 and 3.57 m to melting and refreezing processes. The positive MSA peak at 1.07 m coincided with the depth of the positive NO<sub>3</sub><sup>-</sup> and nssSO<sub>4</sub><sup>2-</sup> peaks. This finding indicates that MSA originating from ocean phytoplankton activity at middle and low latitudes could have been transported to St. 9 with anthropogenic products, including NO<sub>3</sub><sup>-</sup> and  $nssSO_4^{2-}$ . In the snowpack at depths of 0.83, 1.64, and 2.63 m corresponding to summer layers, MSA and/or  $nssSO_4^{2-}$  showed positive peaks, whereas NO<sub>3</sub><sup>-</sup> did not indicate any peaks. Because NO<sub>3</sub><sup>-</sup> peaks did not occur, the air masses containing MSA were not transported from mid-latitudes, which are areas of human activity. Therefore, the positive peaks of MSA at 0.83, 1.64, and 2.63 m could be reflected in sea-to-air DMS emission attributed to the ocean phytoplankton bloom in the NOW polynya.



320

321



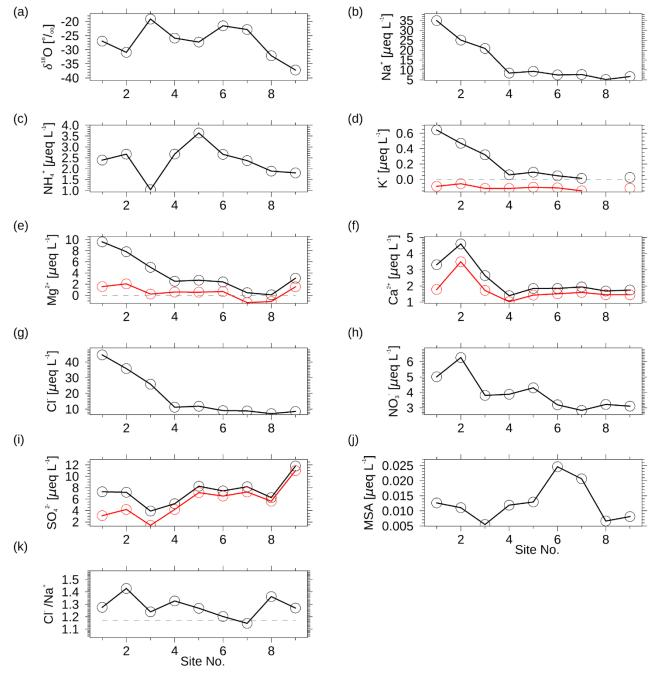
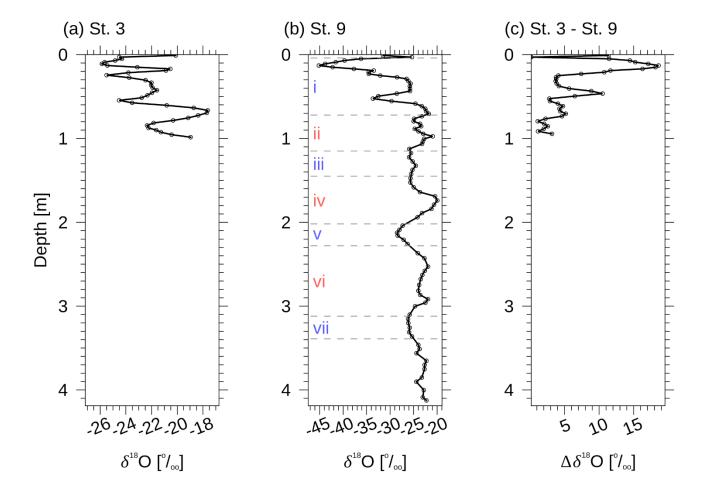


Figure 5: Spatial variability in (a)  $\delta^{18}O$ , (b) Na<sup>+</sup>, (c) NH<sup>+</sup>, (d) K<sup>+</sup>, (e) Mg<sup>2+</sup>, (f) Ca<sup>2+</sup>, (g) Cl<sup>-</sup>, (h) NO<sub>3</sub><sup>-</sup>, (i) SO<sub>4</sub><sup>2-</sup> (j) MSA and (k) Cl<sup>-</sup>/Na<sup>+</sup> concentrations in surface snow. The black and red curves denote the total concentration and non-sea-salt (nss) fractions, respectively. The gray dashed lines in (d), and (e) denote values of 0  $\mu$ eq. L<sup>-1</sup>. The gray dashed lines in (k) denote the Cl<sup>-</sup>/Na<sup>+</sup> ratio in seawater (1.17).



325

326



**Figure 6: Vertical profile of**  $\delta^{18}$ **O.** (a) and (b) show  $\delta^{18}$ O values at St. 3 and St.9, respectively. (c) shows difference between St.3 and St.9 in terms of  $\delta^{18}$ O. i–vii denote seasons from 2019 to 2023. i, iii, v, and vii denote from autumn to winter period from 2022–2023, 2021–2022, 2020–2021, and 2019–2020, respectively. ii, iv, and vi denote from spring to summer in 2022, 2021, and 2020, respectively.



332

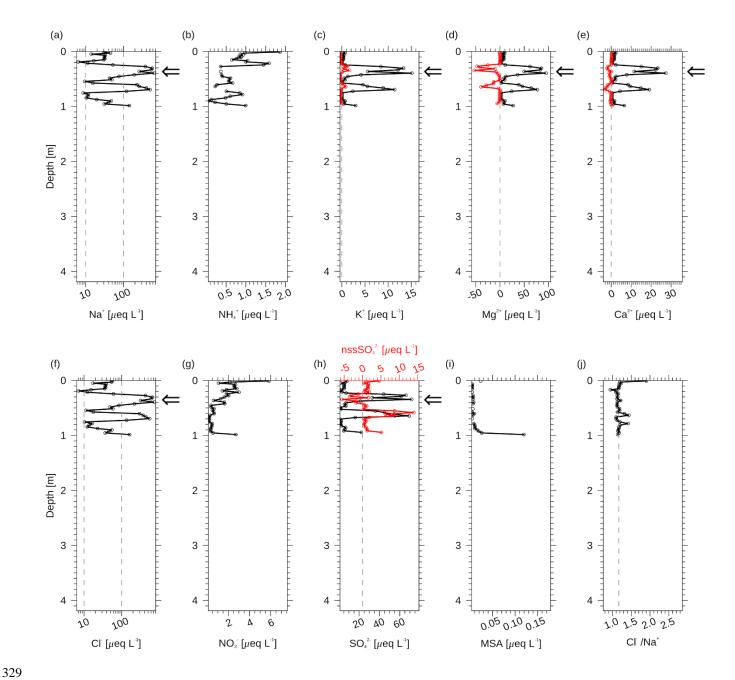


Figure 7: Vertical profiles of (a) Na<sup>+</sup>, (b) NH<sup>+</sup>, (c) K<sup>+</sup>, (d) Mg<sup>2+</sup>, (e) Ca<sup>2+</sup>, (f) Cl<sup>-</sup>, (g) NO<sub>3</sub><sup>-</sup>, (h) SO<sub>4</sub><sup>2-</sup> (i) MSA, and (j) Cl<sup>-</sup>/Na<sup>+</sup> concentrations at St. 3. The black and red curves denote the total concentration and non-sea-salt (nss) fractions, respectively. The gray dashed lines in (a) and (f) denote values of 10, and 100  $\mu$ eq. L<sup>-1</sup>. The gray dashed lines in (c), (d), (e), and (h) denote values of 0  $\mu$ eq. L<sup>-1</sup>. The gray dashed lines in (j) denote Cl<sup>-</sup>/Na<sup>+</sup> in seawater (1.17). The black arrows indicate depths between 0.26 and 0.42 m.



338339

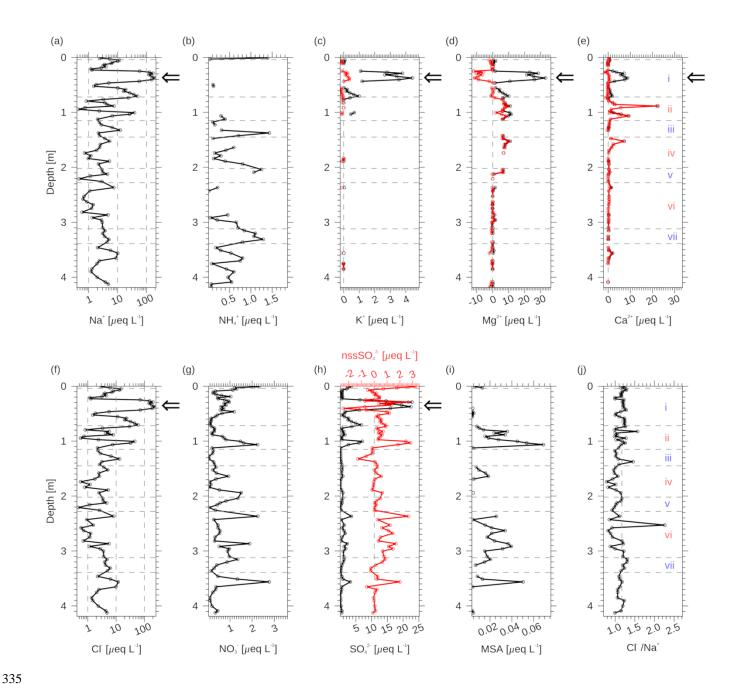


Figure 8: Vertical profiles of (a) Na<sup>+</sup>, (b) NH<sup>+</sup>, (c) K<sup>+</sup>, (d) Mg<sup>2+</sup>, (e) Ca<sup>2+</sup>, (f) Cl<sup>-</sup>, (g) NO<sub>3</sub><sup>-</sup>, (h) SO<sub>4</sub><sup>2-</sup> (i) MSA and (j) Cl<sup>-</sup>/Na<sup>+</sup> concentrations at St. 9. The black and red curves denote the total concentration and non-sea-salt (nss) fractions, respectively. The gray dashed lines in (a) and (f) denote values of 1, 10, and 100  $\mu$ eq. L<sup>-1</sup>. The gray dashed lines in (c), (d), (e), and (h) denote the values of 0  $\mu$ eq. L<sup>-1</sup>. The gray dashed lines in (j) denote Cl<sup>-</sup>/Na<sup>+</sup> in seawater (1.17). i, iii, v, and vii denote from autumn to winter period from 2022–2023, 2021–2022, 2020–2021, and 2019–2020, respectively. ii, iv, and vi



345

346347

348

349350

351

352

353354

355356

357

358359

360361

362

363364

365

366

367

368369



denote from spring to summer period in 2022, 2021, and 2020, respectively. The black arrows indicate depths between 0.26 and 0.42 m.

Table 1. Mean values and standard deviations of several ion species and water stable isotopes between St. 3 and St. 9.

The mean values at St.9 were obtained at depths from 0.00 to 1.01 m.

	Na <sup>+</sup> (µeq L <sup>-1</sup> )	NH <sub>4</sub> <sup>+</sup> (µeq L <sup>-1</sup> )		nssMg <sup>2+</sup> (µeq L <sup>-1</sup> )		MSA (µeq L <sup>-1</sup> )	Cl- (µeq L <sup>-1</sup> )	nssSO <sub>4</sub> <sup>2-</sup> (µeq L <sup>-1</sup> )	NO <sub>3</sub> - (μeq L-1)	Cl <sup>-</sup> /Na <sup>+</sup> (µeq L <sup>-1</sup> )	δ <sup>18</sup> Ο (‰)	δD (‰)	d-excess (‰)
mean(St.3)	133.70	0.61	-0.03	-8.06	-0.46	0.01	155.53	1.51	1.32	1.19	-22.03	-160.27	15.93
std. (St.3)	181.51	0.45	0.46	14.56	0.87	0.02	206.34	3.45	1.19	0.15	2.22	17.58	2.12
mean(St.9)	34.17	0.04	-0.01	-0.64	0.85	0.01	41.37	0.40	0.60	1.17	-29.12	-218.69	14.29
std. (St.9)	54.12	0.22	0.13	5.05	3.67	0.01	65.33	0.92	0.44	0.12	6.46	52.27	2.66

# 3.3 Intense poleward heat and moisture transport events in winter from 2022–2023

The concentrations of  $\delta^{18}O$ , Na<sup>+</sup>, Cl<sup>-</sup>, K<sup>+</sup>, Mg<sup>2+</sup>, SO<sub>4</sub><sup>2-</sup>, and Ca<sup>2+</sup> increased substantially and the nssSO<sub>4</sub><sup>2-</sup>, nssMg<sup>2+</sup>, and nssCa<sup>2+</sup> exhibited negative values at depths from 0.26–0.42 m at St. 3 and St. 9, corresponding to autumn–winter from 2022– 2023 (Fig. 7 and Fig. 8). Because the depth of the positive peaks of  $\delta^{18}$ O and these ions coincided between St. 3 and St. 9, we believe that the snowpacks from 0.26-0.42 m originated from the same precipitation event during the autumn-winter period from 2022–2023. In previous observations of precipitation isotopes in Siorapaluk, the  $\delta^{18}$ O value in precipitation was significantly correlated with the surface air temperature from winter–spring (Matoba et al., 2002). Therefore, the rapid positive increase in  $\delta^{18}$ O at depths from 0.26–0.42 m at St. 3 and St. 9 suggested that the air temperature at our study sites increased during low temperature period, leading to the coldest winter season. Continuous weather monitoring in Siorapaluk revealed that the air temperature increased by more than 0 °C and that the southern component of the wind increased from 5–6 December 2023 (Fig. 9b and c). During this period, the atmospheric pressure gradient at 500 hPa increased along Baffin Bay due to high pressure in Greenland and low pressure in northern Canada, and the southerly wind speed along the western coast of Greenland increased during this period (Fig. 9d and Fig. 10). Consequently, we determined that the rapid increase in  $\delta^{18}$ O at depths from 0.26–0.42 m corresponded to the intense poleward heat and moisture transport event from 5–6 December 2023. The Na<sup>+</sup>, Cl<sup>-</sup>,  $K^+$ ,  $Mg^{2+}$ ,  $SO_4^{2-}$ , and  $Ca^{2+}$  concentrations increased substantially, and  $nssSO_4^{2-}$  exhibited negative values at depths from 0.26– 0.42 m at St. 3 and St. 9 (Fig. 7a, f, j and Fig. 8a, f, j). The Na<sup>+</sup>, Cl<sup>-</sup>, K<sup>+</sup>, Mg<sup>2+</sup>, SO<sub>4</sub><sup>2-</sup>, and Ca<sup>2+</sup> concentrations in frost flowers are comparable to or greater than those in seawater, and the SO<sub>4</sub><sup>2-</sup>/Na<sup>+</sup> ratio of frost flowers is lower than that of seawater (Hara et al., 2017). On the eastern side of the NOW, the southern component of the wind at 2 m a.g.l. increased from 5-6 December 2023, whereas the sea ice concentration remained high (Fig. 9a and c). The increase in the surface wind speed across the sea ice in the NOW from 5-6 December 2023 promoted the atmospheric emission of frost flowers from sea ice, after which the Na<sup>+</sup>, Cl<sup>-</sup>, K<sup>+</sup>, Mg<sup>2+</sup>, SO<sub>4</sub><sup>2-</sup>, and Ca<sup>2+</sup> concentrations increased, and nssSO<sub>4</sub><sup>2-</sup> exhibited negative values at depths from 0.26– 0.42 m at St. 3 and St. 9. We suggest that intense poleward heat and moisture transport events attributed to the high pressure





in Greenland and low pressure in northern Canada caused precipitation, including heavier isotopes and frost flowers on the northwestern coast of Greenland Ice Sheet.

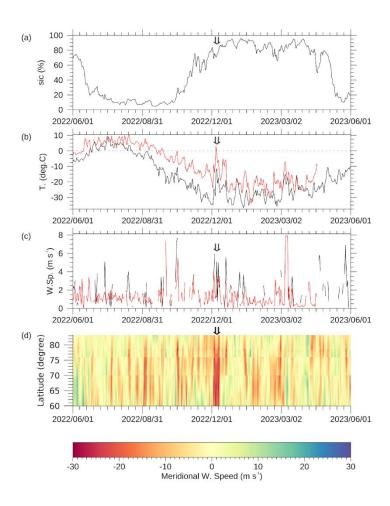


Figure 9: Sea ice and meteorological conditions from April 2022 to April 2023 corresponding to snow depths ranging from 0.00–1.15 m at St. 9. (a) shows the sea ice concentration on the eastern side of NOW. (b) shows the temperature at 2 m a.g.l. in Siorapaluk (red line) and St. 9 (black line). (c) shows the southern component of the wind speed at 2 m a.g.l. in Siorapaluk (red line) and on the eastern side of the NOW (black line). (d) shows the meridional wind speed at 700 hPa along the eastern side of Baffin Bay. The values on the eastern side of the NOW were averaged over 75.0°–80.0°N and 75.0°–65.0°W. The values on the eastern side of Baffin Bay were averaged over 75.0°–65.0°W from 75.0° to 80.0°N, 75.0°–65.0°W from 75.0° to 80.0°N, 75.0°–65.0°W from 75.0° to 80.0°N. The positive and negative values of the meridional wind speed are the southern and northern parts of the wind, respectively. The black arrows denote the date from 5–6 December 2023.





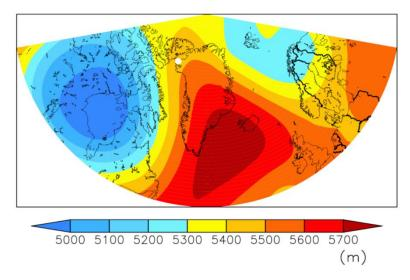


Figure 10: Geopotential height at 500 hPa averaged from 5 to 6 December 2022. The white circle indicates the location of St.9.

#### 4 Conclusion

We conducted glaciological observations from 9–11 April 2023 on the western side of Prudhoe Land in northwestern Greenland to elucidate the source conditions and transportation processes of water vapor and aerosols along the northwestern coast of Greenland facing the NOW. We estimated the age of the snowpack at St. 9, which is located at the inland of the western side of Prudhoe Land, using  $\delta^{18}$ O, d-excess, MSA, and snow stratigraphy to analyze the seasonal variations in chemical substances in the snowpack. The dating of the snowpack at St. 9 revealed that the layer at a depth of 4.20 m corresponded to 3.5 years. The average annual accumulation at St. 9 was 0.49 m w.eq. yr<sup>-1</sup>.

The surface snow and snowpack on the western side of Prudhoe Land were greatly influenced by local phenomena around the NOW. The  $\delta^{18}$ O values and chemical substances in surface snow revealed that water vapor and aerosols were directly transported from the southern coast, which faces the NOW, to the northern inland area of the western side of Prudhoe Land by southerly winds. The nssMg<sup>2+</sup> and nssCa<sup>2+</sup> in the snowpack on the western side of Prudhoe Land showed positive peaks in spring and summer. The spring peaks of nssMg<sup>2+</sup> and nssCa<sup>2+</sup> could stem from remote dust in Asia and North Africa. The summer peaks of nssMg<sup>2+</sup> and nssCa<sup>2+</sup> could originate from local dust around the coast of northwestern Greenland. The seasonal variation in MSA in the snowpack showed positive peaks from winter–spring and summer. The winter–spring peaks of MSA originated from spring phytoplankton blooms in the mid-latitude ocean and were transported to the west side of Prudhoe Land with anthropogenic aerosols such as NO<sub>3</sub><sup>-</sup> and nssSO<sub>4</sub><sup>2-</sup>, which originate from fossil fuel combustion. In contrast,





the summer MSA peaks likely originated from sea-to-air DMS emission following a phytoplankton bloom in the NOW polynya, which is one of the most biologically productive marine areas of the Arctic Ocean. The snowpack on the western side of Prudhoe Land contained other signals of ocean biological activity, such as autumn—winter peaks of NH<sub>4</sub><sup>+</sup>, which could have originated from the atmospheric emission of ammonia gas from the NOW during the decline and death phases of organisms in the NOW polynya. Another characteristic of the snowpack on the western side of Prudhoe Land was the negative peaks of nssSO<sub>4</sub><sup>2-</sup> from autumn—winter. This could be attributed to the atmospheric emission of frost flowers, which exhibit depletion of sulfate relative to that in seawater, from newly formed sea ice in the NOW.

The snowpack on the western side of Prudhoe Land was also influenced by large-scale atmospheric circulation. The intense poleward heat and moisture transport event resulting from a high atmospheric pressure gradient at 500 hPa along Baffin Bay caused snowfall, including high  $\delta^{18}$ O, Na<sup>+</sup>, Cl<sup>-</sup>, K<sup>+</sup>, Mg<sup>2+</sup>, SO<sub>4</sub><sup>2-</sup>, and Ca<sup>2+</sup> values and low nssSO<sub>4</sub><sup>2-</sup> values during the coldest winter season. This suggested that the air mass, including large amount of water vapor, was transported from the mid-latitude ocean poleward and mixed with frost flowers over the NOW.

The snowpacks on the western side of Prudhoe Land close to the NOW polynya contained aerosols from distant sources, such as remote dust and anthropogenic aerosols, in spring, whereas they also contained aerosols from local sources such as ocean biological activity and frost flowers in the NOW and local dust around the coast of northwestern Greenland during other seasons, unlike the inland of the Greenland Ice Sheet. Moreover, we noted that the snowpacks on the western side of the Prudhoe Land was able to trace the poleward heat and moisture transport event along Baffin Bay during winter.

Arctic climate warming caused decreases in the sea ice thickness and concentration over the last few decades in the NOW and could influence clouds and precipitation following changes in sea ice and biological activities in the NOW. We found for the first time that the environmental changes in the NOW can be elucidated by the snowpack and ice core on the western side of the Prudhoe Land. We suggest that the chemical substances in the deeper ice core from the western side of Prudhoe Land could help explain the multidecadal variations in the sea ice, biological activities, and related water and aerosol circulation around the NOW and could develop to understand the accurate future projections of environmental change in this region.

### Code availability

- Data analyses were performed using Interactive Data Language (IDL) (version 8.7.1) developed by Exelis Visual
- 429 Information Solutions, Boulder, Colorado. Map figures were generated using Generic-Mapping Tools (GMT) (version 6.1.0)
- 430 (https://www.generic-mapping-tools.org/) and Quantum Geographic Information System (QGIS) (https://qgis.org/).

#### Data availability

- The data used in this are available from the Hokkaido University Collection of Scholarly and Academic Papers (HUSCAP)
- 433 (http://hdl.handle.net/2115/94742). The AWS data are available from the Arctic Data archive System (ADS)





- 434 (https://ads.nipr.ac.jp/data/meta/A20241031-013). The ERA5 data are available from the Copernicus Climate Change Service
- 435 (C3S) Climate Data Store (https://cds.climate.copernicus.eu/#!/search?text=ERA5&type=dataset). The Landsat-8 image is
- provided by United States Geological Survey (https://earthexplorer.usgs.gov/). The Greenland Mapping Project 2 (GIMP-2)
- 437 digital elevation model version 2 is provided by the National Snow and Ice Data Center (NSIDC) (https://nsidc.org/data/nsidc-
- 438 0715/versions/2).

#### 439 Author contributions

- 440 Y.K. and S.M. designed this study. Y.K., M.M, T.K, and H.I. collected and processed the snow samples during the field
- 441 observations. Y.K. and S.M. analyzed water stable isotopes and chemical substances in the snow samples. Y.K. analyzed the
- 442 meteorological and sea ice data. Y.K. and S.M. wrote the manuscript draft. Y.I. reviewed the manuscript.

#### 443 Competing interests

The contact author has declared that none of the authors has any competing interests.

# 445 Acknowledgement

- We thank Dr. Akihiro Hashimoto of Meteorological Research Institute, Japan Meteorological Agency, for the provided
- 447 ground support in Japan. We also thank Yusuke Kakuhata and Ikuo Oshima for the valuable suggestions for the field
- 448 observations.

444

### 449 Financial support

- This study was supported in part by (1) the Japan Society for the Promotion of Science (JSPS) KAKENHI grant 22J10351,
- 451 18H05292, 23H00511, and 24H00757, (2) the Arctic Challenge for Sustainability (ArCS II) Project (JPMXD1420318865),
- 452 and (3) the National Institute of Polar Research through Special Collaboration Project no. B24-02.

#### 453 References

- 454 Akers, P. D., Kopec, B. G., Mattingly, K. S., Klein, E. S., Causey, D., and Welker, J. M.: Baffin Bay sea ice extent and synoptic
- 455 moisture transport drive water vapor isotope ( $\delta^{18}$ O,  $\delta^{2}$ H, and deuterium excess) variability in coastal northwest Greenland,
- 456 Atmos. Chem. Phys., 20, 13929–13955, https://doi.org/10.5194/acp-20-13929-2020, 2020.





- 457 Amino, T., Iizuka, Y., Matoba, S., Shimada, R., Oshima, N., Suzuki, T., Ando, T., Aoki, T., and Fujita, K.: Increasing dust
- emission from ice free terrain in southeastern Greenland since 2000, Polar Science, 27, 100599,
- 459 https://doi.org/10.1016/j.polar.2020.100599, 2021.
- 460 Bales, R. C., McConnell, J. R., Mosley Thompson, E., and Csatho, B.: Accumulation over the Greenland ice sheet from
- 461 historical and recent records, J. Geophys. Res., 106, 33813–33825, https://doi.org/10.1029/2001JD900153, 2001.
- 462 Barber, D. G. and Massom, R. A.: The Role of Sea Ice in Arctic and Antarctic Polynyas, Polynyas: Windows to the World.,
- edited by: Smith, W. O. and Barber, D. G., Elsevier, Amsterdam, 1–54 pp., 2007.
- 464 Becagli, S., Lazzara, L., Marchese, C., Dayan, U., Ascanius, S. E., Cacciani, M., Caiazzo, L., Di Biagio, C., Di Iorio, T., Di
- 465 Sarra, A., Eriksen, P., Fani, F., Giardi, F., Meloni, D., Muscari, G., Pace, G., Severi, M., Traversi, R., and Udisti, R.:
- 466 Relationships linking primary production, sea ice melting, and biogenic aerosol in the Arctic, Atmospheric Environment,
- 467 136, 1–15, https://doi.org/10.1016/j.atmosenv.2016.04.002, 2016.
- Burgess, E. W., Forster, R. R., Box, J. E., Mosley-Thompson, E., Bromwich, D. H., Bales, R. C., and Smith, L. C.: A spatially
- 469 calibrated model of annual accumulation rate on the Greenland Ice Sheet (1958-2007), J. Geophys. Res., 115,
- 470 2009JF001293, https://doi.org/10.1029/2009JF001293, 2010.Cadle, R. D.: Formation and Chemical Reactions of
- 471 Atmospheric Particles, Journal of Colloid and Interface Science, 39, 25–31, https://doi.org/10.1016/0021-9797(72)90138-
- 472 5, 1972.
- 473 Charlson, R. J., Lovelock, J. E., Andreae, M. O., and Warren, S. G.: Oceanic phytoplankton, atmospheric sulphur, cloud albedo
- and climate, Nature, 326, 655–661, https://doi.org/10.1038/326655a0, 1987.
- 475 Delmas, R., Briat, M., and Legrand, M.: Chemistry of south polar snow, J. Geophys. Res. Oceans, 87, 4314-4318,
- 476 https://doi.org/10.1029/JC087iC06p04314, 1982.
- 477 Dibb, J. E., Whitlow, S. I., and Arsenault, M.: Seasonal variations in the soluble ion content of snow at Summit. Greenland:
- 478 Constraints from three years of daily surface snow samples, Atmospheric Environment, 41, 5007–5019,
- 479 https://doi.org/10.1016/j.atmosenv.2006.12.010, 2007.
- 480 Dobashi, T.: Role of marine nitrogen-fixing organisms in the formation of atmospheric reactive nitrogen, theses (doctoral),
- 481 Hokkaido University, Sapporo, 85 pp., 2023.
- 482 Drab, E., Gaudichet, A., Jaffrezo, J. L., and Colin, J. L.: Mineral particles content in recent snow at Summit (Greenland),
- 483 Atmospheric Environment, 36, 5365–5376, https://doi.org/10.1016/S1352-2310(02)00470-3, 2002.
- 484 Du, Z., Xiao, C., Zhang, Q., Li, C., Wang, F., Liu, K., and Ma, X.: Climatic and environmental signals recorded in the EGRIP
- snowpit, Greenland, Environ Earth Sci, 78, 170, https://doi.org/10.1007/s12665-019-8177-4, 2019.
- 486 Dumont, D., Gratton, Y., and Arbetter, T. E.: Modeling the Dynamics of the North Water Polynya Ice Bridge, J. Phys.
- 487 Oceanogr., 39, 1448–1461, https://doi.org/10.1175/2008JPO3965.1, 2009.
- 488 Fischer, H. and Wagenbach, D.: Large-scale spatial trends in recent firn chemistry along an east-west transect through central
- 489 Greenland, Atmos. Environ., 30, 3227–3238, https://doi.org/10.1016/1352-2310(96)00092-1, 1996.





- 490 Fuhrer, K. and Legrand, M.: Continental biogenic species in the Greenland Ice Core Project ice core: Tracing back the biomass
- 491 history of the North American continent, J. Geophys. Res., 102, 26735–26745, https://doi.org/10.1029/97JC01299, 1997.
- 492 Hara, K., Matoba, S., Hirabayashi, M., and Yamasaki, T.: Frost flowers and sea-salt aerosols over seasonal sea-ice areas in
- 493 northwestern Greenland during winter–spring, Atmos. Chem. Phys., 17, 8577–8598, https://doi.org/10.5194/acp-17-8577-
- 494 2017, 2017.
- 495 Hastings, M. G., Steig, E. J., and Sigman, D. M.: Seasonal variations in N and O isotopes of nitrate in snow at Summit,
- 496 Greenland: Implications for the study of nitrate in snow and ice cores, J. Geophys. Res., 109, 2004JD004991,
- 497 https://doi.org/10.1029/2004JD004991, 2004.
- 498 Hersbach, H., Bell, B., Berrisford, P., Hirahara, S., Horányi, A., Muñoz-Sabater, J., Nicolas, J., Peubey, C., Radu, R., Schepers,
- 499 D., Simmons, A., Soci, C., Abdalla, S., Abellan, X., Balsamo, G., Bechtold, P., Biavati, G., Bidlot, J., Bonavita, M., De
- 500 Chiara, G., Dahlgren, P., Dee, D., Diamantakis, M., Dragani, R., Flemming, J., Forbes, R., Fuentes, M., Geer, A.,
- Haimberger, L., Healy, S., Hogan, R. J., Hólm, E., Janisková, M., Keeley, S., Laloyaux, P., Lopez, P., Lupu, C., Radnoti,
- 502 G., De Rosnay, P., Rozum, I., Vamborg, F., Villaume, S., and Thépaut, J.: The ERA5 global reanalysis, Quart J Royal
- 503 Meteoro Soc, 146, 1999–2049, https://doi.org/10.1002/qj.3803, 2020.
- Ingram, R. G., Bâcle, J., Barber, D. G., Gratton, Y., and Melling, H.: An overview of physical processes in the North Water,
- Deep Sea Research Part II: Topical Studies in Oceanography, 49, 4893-4906, https://doi.org/10.1016/S0967-
- 506 0645(02)00169-8, 2002.
- 507 Ito, H.: Wind Through a Channel—Surface Wind Measurements in Smith Sound and Jones Sound in Northern Baffin Bay, J.
- 508 Appl. Meteor. and Clim., 21, 1053–1062, https://doi.org/10.1175/1520-0450(1982)021<1053:WTACWM>2.0.CO;2,
- 509 1982.
- Jaffrezo, J.-L., Davidson, C. I., Legrand, M., and Dibb, J. E.: Sulfate and MSA in the air and snow on the Greenland Ice Sheet,
- J. Geophys. Res. Atom., 99, 1241–1253, https://doi.org/10.1029/93JD02913, 1994.
- 512 Johnsen, S. J., Dansgaard, W., and White, J. W. C.: The origin of Arctic precipitation under present and glacial conditions,
- 513 Tellus B, 41B, 452–468, https://doi.org/10.1111/j.1600-0889.1989.tb00321.x, 1989.
- 514 Kerminen, V.-M., Teinilä, K., and Hillamo, R.: Chemistry of sea-salt particles in the summer Antarctic atmosphere,
- 515 Atmospheric Environment, 34, 2817–2825, https://doi.org/10.1016/S1352-2310(00)00089-3, 2000.
- 516 Kjær, H. A., Zens, P., Black, S., Lund, K. H., Svensson, A., and Vallelonga, P.: Canadian forest fires, Icelandic volcanoes and
- 517 increased local dust observed in six shallow Greenland firn cores, Clim. Past, 18, 2211–2230, https://doi.org/10.5194/cp-
- 518 18-2211-2022, 2022.
- 519 Klein, B., LeBlanc, B., Mei, Z.-P., Beret, R., Michaud, J., Mundy, C.-J., Von Quillfeldt, C. H., Garneau, M.-È., Roy, S.,
- 520 Gratton, Y., Cochran, J. K., Bélanger, S., Larouche, P., Pakulski, J. D., Rivkin, R. B., and Legendre, L.: Phytoplankton
- 521 biomass, production and potential export in the North Water, Deep Sea Research Part II: Topical Studies in Oceanography,
- 522 49, 4983–5002, https://doi.org/10.1016/S0967-0645(02)00174-1, 2002.





- 523 Kopec, B. G., Feng, X., Posmentier, E. S., and Sonder, L. J.: Seasonal Deuterium Excess Variations of Precipitation at Summit,
- Greenland, and their Climatological Significance, JGR Atmospheres, 124, 72–91, https://doi.org/10.1029/2018JD028750,
- 525 2019.
- 526 Kuramoto, T., Goto-Azuma, K., Hirabayashi, M., Miyake, T., Motoyama, H., Dahl-Jensen, D., and Steffensen, J. P.: Seasonal
- 527 variations of snow chemistry at NEEM, Greenland, Ann. Glaciol., 52, 193-200,
- 528 https://doi.org/10.3189/172756411797252365, 2011.
- 529 Kurita, N.: Origin of Arctic water vapor during the ice-growth season: ORIGIN OF ARCTIC MOISTURE, Geophys. Res.
- 530 Lett., 38, n/a-n/a, https://doi.org/10.1029/2010GL046064, 2011.
- Kurosaki, Y., Matoba, S., Iizuka, Y., Niwano, M., Tanikawa, T., Ando, T., Hori, A., Miyamoto, A., Fujita, S., and Aoki, T.:
- Reconstruction of Sea Ice Concentration in Northern Baffin Bay Using Deuterium Excess in a Coastal Ice Core From the
- 533 Northwestern Greenland Ice Sheet, JGR Atmospheres, 125, e2019JD031668, https://doi.org/10.1029/2019JD031668, 2020.
- 534 Kurosaki, Y., Matoba, S., Iizuka, Y., Fujita, K., and Shimada, R.: Increased oceanic dimethyl sulfide emissions in areas of sea
- ice retreat inferred from a Greenland ice core, Commun Earth Environ, 3, 327, https://doi.org/10.1038/s43247-022-00661-
- 536 w, 2022.
- 537 Legrand, M. and Mayewski, P.: Glaciochemistry of polar ice cores: A review, Reviews of Geophysics, 35, 219-243,
- 538 https://doi.org/10.1029/96RG03527, 1997.
- 539 Marchese, C., Albouy, C., Tremblay, J.-É., Dumont, D., D'Ortenzio, F., Vissault, S., and Bélanger, S.: Changes in
- 540 phytoplankton bloom phenology over the North Water (NOW) polynya: a response to changing environmental conditions,
- 541 Polar Biol., 40, 1721–1737, 2017.
- 542 Matoba, S. and Yamasaki, T.: Sea ice outflow damage to fishery in Qaanaaq, northwestern Greenland in December 2016. –
- 543 Changes of the livelihood associated with social and environmental changes [in Japanese], Ann. Rep. Snow Ice Sheet
- 544 Hokkaido, 37, 51–54, 2018.
- 545 Matoba, S., Yamasaki, T., and Motoyama, H.: Meteorological observation and chemical compositions of precipitation during
- 546 the winter and spring season in 1997/98 at Siorapaluk, northwetern Greenland, Bull. Glaciol. Res., 19, 25–31, 2002.
- 547 Matoba, S., Yamasaki, T., Miyahara, M., and Motoyama, H.: Spatial variations of δ18O and ion species in the snowpack of
- 548 the northwestern Greenland ice sheet, Bulletin of Glacier Research, 32, 79–84, https://doi.org/10.5331/bgr.32.79, 2014.
- 549 Matoba, S., Motoyama, H., Fujita, K., Yamasaki, T., Minowa, M., Onuma, Y., Komuro, Y., Aoki, T., Yamaguchi, S., Sugiyama,
- 550 S., and Enomoto, H.: Glaciological and meteorological observations at the SIGMA-D site, northwestern Greenland Ice
- Sheet, Bulletin of Glacier Research, 33, 7–14, https://doi.org/10.5331/bgr.33.7, 2015.
- 552 Matoba, S., Niwano, M., Tanikawa, T., Iizuka, Y., Yamasaki, T., Kurosaki, Y., Aoki, T., Hashimoto, A., Hosaka, M., and
- Sugiyama, S.: Field activities at the SIGMA-A site, northwestern Greenland Ice Sheet, 2017, Bull. Glaciol. Res., 36, 15-
- 554 22, https://doi.org/10.5331/bgr.18R01, 2018.
- 555 Matoba, S., Kurosaki, Y., and Miyazaki, Y.: Siorapaluk AWS data from 2021to 2024, 0.00, Arctic Data archive System (ADS)
- 556 [dataset], Japan, 2024.





- 557 Matsui, H., Kawai, K., Tobo, Y., Iizuka, Y., and Matoba, S.: Increasing Arctic dust suppresses the reduction of ice nucleation
- in the Arctic lower troposphere by warming, npj Clim Atmos Sci, 7, 266, https://doi.org/10.1038/s41612-024-00811-1,
- 559 2024.
- 560 Melling, H., Gratton, Y., and Ingram, G.: Ocean circulation within the North Water polynya of Baffin Bay, Atmosphere-Ocean,
- 39, 301–325, https://doi.org/10.1080/07055900.2001.9649683, 2001.
- 562 Merlivat, L. and Jouzel, J.: Global climatic interpretation of the deuterium-oxygen 18 relationship for precipitation, J. Geophys.
- Res., 84, 5029–5033, https://doi.org/10.1029/JC084iC08p05029, 1979.
- Monroe, E. E., Taylor, P. C., and Boisvert, L. N.: Arctic Cloud Response to a Perturbation in Sea Ice Concentration: The North
- Water Polynya, JGR Atmospheres, 126, e2020JD034409, https://doi.org/10.1029/2020JD034409, 2021.
- 566 Mosher, B. W., Winkler, P., and Jaffrezo, J.-L.: Seasonal aerosol chemistry at Dye 3, Greenland, Atmospheric Environment.
- Part A. General Topics, 27, 2761–2772, https://doi.org/10.1016/0960-1686(93)90308-L, 1993.
- 568 Mysak, L. A. and Huang, F.: A Latent-and Sensible-Heat Polynya Model for the North Water, Northern Baffin Bay, J. Phys.
- Oceanogr., 22, 596–608, https://doi.org/10.1175/1520-0485(1992)022<0596:ALASHP>2.0.CO;2, 1992.
- 570 Nagatsuka, N., Goto-Azuma, K., Tsushima, A., Fujita, K., Matoba, S., Onuma, Y., Dallmayr, R., Kadota, M., Hirabayashi, M.,
- Ogata, J., Ogawa-Tsukagawa, Y., Kitamura, K., Minowa, M., Komuro, Y., Motoyama, H., and Aoki, T.: Variations in
- 572 mineralogy of dust in an ice core obtained from northwestern Greenland over the past 100 years, Clim. Past, 17, 1341–
- 573 1362, https://doi.org/10.5194/cp-17-1341-2021, 2021.
- 574 Nakazawa, F., Nagatsuka, N., Hirabayashi, M., Goto-Azuma, K., Steffensen, J. P., and Dahl-Jensen, D.: Variation in recent
- annual snow deposition and seasonality of snow chemistry at the east Greenland ice core project (EGRIP) camp, Greenland,
- 576 Polar Science, 27, 100597, https://doi.org/10.1016/j.polar.2020.100597, 2021.
- 577 NEEM community members: Eemian interglacial reconstructed from a Greenland folded ice core, Nature, 493, 489–494,
- 578 https://doi.org/10.1038/nature11789, 2013.
- 579 Odate, T., Hirawake, T., Kudoh, S., Klein, B., LeBlanc, B., and Fukuchi, M.: Temporal and spatial patterns in the surface-
- water biomass of phytoplankton in the North Water, Deep Sea Research Part II: Topical Studies in Oceanography, 49,
- 581 4947–4958, https://doi.org/10.1016/S0967-0645(02)00172-8, 2002.
- 582 Osterberg, E. C., Hawley, R. L., Wong, G., Kopec, B., Ferris, D., and Howley, J.: Coastal ice-core record of recent northwest
- Greenland temperature and sea-ice concentration, J. Glaciol., 61, 1137–1146, https://doi.org/10.3189/2015JoG15J054,
- 584 2015.
- 585 Oyabu, I., Matoba, S., Yamasaki, T., Kadota, M., and Iizuka, Y.: Seasonal variations in the major chemical species of snow at
- the South East Dome in Greenland, Polar Science, 10, 36–42, https://doi.org/10.1016/j.polar.2016.01.003, 2016.
- 587 Rankin, A. M., Wolff, E. W., and Martin, S.: Frost flowers: Implications for tropospheric chemistry and ice core interpretation,
- J.-Geophys.-Res., 107, https://doi.org/10.1029/2002JD002492, 2002.
- 589 Rankin, A. M., Wolff, E. W., and Mulvaney, R.: A reinterpretation of sea-salt records in Greenland and Antarctic ice cores?,
- 590 Ann. Glaciol., 39, 276–282, https://doi.org/10.3189/172756404781814681, 2004.





- 591 Richardson, C.: Phase Relationships in Sea Ice as a Function of Temperature, J. Glaciol., 17, 507-519,
- 592 https://doi.org/10.3189/S0022143000013770, 1976.
- 593 Steffen, K. and Ohmura, A.: Heat Exchange and Surface Conditions in North Water Northern Baffin Bay, Ann. Glaciol., 6,
- 594 178–181, https://doi.org/10.3189/1985AoG6-1-178-181, 1985.
- 595 Steffensen, J. P.: Analysis of the Seasonal Variation in Dust, Cl<sup>-</sup>, NO<sub>3</sub><sup>-</sup>, and SO<sub>4</sub><sup>2-</sup> in Two Central Greenland Firn Cores,
- 596 Ann. Glaciol., 10, 171–177, https://doi.org/10.3189/S0260305500004389, 1988.
- 597 Uemura, R., Matsui, Y., Yoshimura, K., Motoyama, H., and Yoshida, N.: Evidence of deuterium excess in water vapor as an
- 598 indicator of ocean surface conditions, J. Geophys. Res., 113, 2008JD010209, https://doi.org/10.1029/2008JD010209, 2008.
- 599 Vincent, R. F.: A Study of the North Water Polynya Ice Arch using Four Decades of Satellite Data, Sci Rep, 9, 20278,
- 600 https://doi.org/10.1038/s41598-019-56780-6, 2019.
- 601 Whitlow, S., Mayewski, P. A., and Dibb, J. E.: A comparison of major chemical species seasonal concentration and
- accumulation at the South Pole and summit, Greenland, Atmospheric Environment. Part A. General Topics, 26, 2045–
- 603 2054, https://doi.org/10.1016/0960-1686(92)90089-4, 1992.
- Wilson, T. R. S.: Salinity and the major elements of sea water, edited by: Riley, J. P. and Skittow, G., Chemical Oceanography,
- 605 London, Academic Press., 365–413 pp., 1975.
- 606 Wolff, E. W., Rankin, A. M., and Röthlisberger, R.: An ice core indicator of Antarctic sea ice production?, Geophysical
- 607 Research Letters, 30, 2003GL018454, https://doi.org/10.1029/2003GL018454, 2003.